Scientific Papers. Series E. Land Reclamation, Earth Observation & Surveying, Environmental Engineering. Vol. XII, 2023
Print ISSN 2285-6064, CD-ROM ISSN 2285-6072, Online ISSN 2393-5138, ISSN-L 2285-6064

SUPERIOR PHOTOGRAMMETRIC PRODUCTS USING DIRECT GEOREFERENCING, LIDAR DATA AND PRECISE TRANSFORMATIONS

Daniel ILIE[1, 2, 3], Constantin MOLDOVEANU[1], Octavian Laurentiu BALOTA[2, 4]

[1]Technical University of Civil Engineering of Bucharest,
112-124 Lacul Tei Blvd, District 2, Bucharest, Romania
[2]Romanian Society of Photogrammetry and Remote Sensing,
124 Lacul Tei Blvd, District 2, Bucharest, Romania
[3]Terra Advanced Technologies SRL, 149 Bahluiului Street, Ploiesti, Romania
[4]University of Agronomic Sciences and Veterinary Medicine of Bucharest,
59 Marasti Blvd, District 1, Bucharest, Romania

Corresponding author email: danielilie17@yahoo.com

Abstract

The current research presents the way to obtain direct georeferencing of photogrammetric imagery and to obtain rigorously georeferenced orthophoto plans without using ground control points. The direct georeferencing procedure is studied in Romania`s atypical coordinate systems (planimetric system based on an ellipsoid different than GRS80 and a vertical system of normal elevations, different than the ellipsoidal elevations used in GNSS technology), but it can also be applied to other systems of coordinates. To generate superior photogrammetric products, an innovative orthorectification methodology based on LIDAR data acquired simultaneously with photogrammetric images is presented. LIDAR data is also acquired by a direct georeferencing procedure and transformed with high precision using an application designed for this purpose. Therefore, a much faster way to generate orthophoto plans is presented, with lower production costs, without a substantial loss of the positional quality of the final product. Finally, there is presented the first stereo restitution project in Romania using small size images, acquired with a UAV system by direct georeferencing. The focus on the atypical case of Romania underlines the innovative features of this research.

Key words*: direct georeferencing, orthorectification, LIDAR, UAV stereo restitution.*

INTRODUCTION

The accelerated development of unmanned aerial vehicle (UAV) photogrammetric systems in recent years and their widespread distribution demonstrate the usefulness of research in this area. Current research reveals how superior photogrammetric products can be obtained through direct georeferencing (DG) orthorectification based on Light Detection and Ranging (LIDAR) data, and precise transformations.

Direct georeferencing (DG) in the field of photogrammetry has been one of the topics that has concerned many geodetic researchers in the last decades (Chiang et al., 2012). A comprehensive presentation of this subject was made in the review article published by Correia et al. (2022). The problem of accurate georeferencing of photogrammetric products is currently solved indirectly by using ground control points (GCP) and the bundle block adjustment (BBA) method in aerotriangulation. The development of in-flight positioning sensors (Global Navigation Satellite System (GNSS) antennas, Inertial Measurement Unit (IMU) sensors, Inertial Navigation System (INS), Synchronized Position Attitude Navigation (SPAN) system, etc.) has opened the possibility to identify better positioning solutions than indirect georeferencing through GCPs. The development of the SPAN system paved the way for direct georeferencing, and the first tests were carried out on the photogrammetric airplanes as early as 2007 by the company that invented this system, NovAtel (Development Team of NovAtel, 2007).

Currently, there are several studies carried out recently in the field of direct georeferencing, but also comparisons between the various methods approached (Gómez-Gutiérrez, 2022), which showed that low-cost photogrammetric systems cannot achieve satisfactory results for geodetic works (Essel et al., 2022). In the field of UAV

systems, several studies on direct georeferencing are known. However, most of them have a much poorer final positioning accuracy than that pursued in the current research (Salas López et al., 2022; Teppati Losè et al., 2020; Thiab & Seker, 2022). Even for UAV systems with built-in Real Time Kinematics (RTK) technology, the direct georeferencing error relative to the unit pixel is approximately ten times greater (Przybilla et al., 2020). There are also studies that propose a hybrid approach to DG by using a reduced number of GCPs (Liu et al., 2022). Rigorous calibration of imaging systems for DG is another topic of current research (Kordić et al., 2020). A part of the principles required for DG, such as camera calibration based on images acquired in a grid pattern, are presented in some research articles (Hutton et al., 2020). Another type of hybrid DG is based on the acquisition of highly accurate LIDAR data alongside the optical data. Finally, the optical data is georeferenced by correlation with the LIDAR data, but the LIDAR data is georeferenced with the help of ground targets, resulting in an indirect georeferencing (Haala et al., 2022).

Another field where similar research has not been identified is the realization of directly georeferenced stereo restitution projects, with small-sized images taken from low altitudes.

The aim of this research was to obtain directly georeferenced orthophoto for stereo restitution and rigorously georeferenced orthophoto plans without using GCP. The assumed goal was to obtain a maximum error of 1-2 GSD (Ground Sample Distance) for DG products.

The DG procedure will be studied mainly in the national coordinate systems of Romania (the 1970 Stereographic planimetric system and the Black Sea 1975 altimetric system), but it can be reproduced in any other coordinate systems.

The procedure for obtaining direct georeferencing, through its method of implementation, is itself an innovative element. The focus on the atypical case of Romania (planimetric system based on a different ellipsoid and a system of normal heights, different from those used according to the GNSS technology) underlines the innovative feature of this research. Thereby, the aim is to obtain orthophoto plans much faster, with production costs as low as possible, without a substantial loss of the positional quality of the final product. In conclusion, no research is known about direct georeferencing achieved within the assumed accuracy limit. Moreover, there are no known direct georeferencing studies carried out in Romania's national coordinate systems. It should be noted that there are implications of local systems in which direct georeferencing is carried out. These implications will be developed in current research. There is also no global research on orthorectification based on directly georeferenced LIDAR data, and even less in Romania's coordinate systems. The lack of methods for accurately transforming LIDAR data files makes this a difficult topic to approach. In practice, in the best case scenario, LIDAR data files are transformed with an error of 0.1-0.5m in 3D (Ilie et al., 2022).

All these aspects lead to the usefulness of this research with direct applicability to photogrammetric works in Romania. However, the principles that will be stated can be adapted for other photogrammetric systems, respectively for other coordinate systems.

MATERIALS AND METHODS

1. Equipment used

In terms of georeferencing, the integrator of the equipment used, UAV-M600-VLP32c-SonyA7RII, Phoenix LiDAR Systems LLC (PLS), proposes the use of 10 GCPs for a flight area of approximately 1 km^2 (100 ha) (Development Team of PLS, 2018). Also in the cited report, it is mentioned that the number of points on the ground increases in the context where more flights are used on the surface of 1 km^2. In the case of the UAV-M600-VLP32c-SonyA7RII system, for a height of up to 120m, the surface of 1 km^2 can be covered by at least 4 flight missions. In this case, the number of GCPs would increase exponentially, in the context in which they would also be needed in connecting areas between flights.

As a result of the experiments carried out, several essential elements were found for obtaining a system capable of DG. The main elements that have an important role in direct georeferencing and the minimum requirements regarding their technical capacity will be highlighted. The present study was carried out with the help of an integrated system for

simultaneous acquisition of LIDAR and optical data. The system is composed of a Velodyne UltraPuck LIDAR sensor (VLP 32c), nadiral oriented (Field Of View 40°/360°), with a maximum recording capacity of 1.2 mil. points/s, a maximum range of 200 m and an internal accuracy of ± 3 cm. The optical sensor is a Sony A7RII camera, nadiral oriented, with a resolution of 42 MB pixels and a focal length of approximately 20.79 mm.

2. Technical requirements

The system used must have an IMU dedicated to photogrammetric sensors with an update rate of at least 125Hz. The SPAN INS technology developed by NovAtel (Hexagon), which combines GNSS data and INS data, is also an essential element for a DG system (Development Team of NovAtel, 2020).

Complementarily, the scanning system must have its own GNSS receiver, capable of receiving satellite data from NAVSTAR (L1/L2/L2C/L5), GLONASS (L1/L2), Galileo (E1/E5a/E5b) and BeiDou (B1/B2). For accurate georeferencing it is important that the GNSS antenna to be equipped with multipath error filtering technology (*choke rings*) (Development Team of NovAtel, 2022).

The essential element to have a DG system consist of a rigid mounting of sensors to the IMU unit, but also of their precise calibration. To assure the quality of the LIDAR data, it is necessary that the vibrations generated by the engines and propellers are attenuated by rubber dampers, and thus transformed into vibrations that can be recorded by IMU.

For a correct georeferencing it is necessary that the flight platform is stable during the flight in order not to induce errors in the georeferencing. In this case, the aerial platform is the DJI Matrice M600 PRO, a hexacopter with a weight of 13.5 kg (including the onboard sensors), which ensures a smooth flight, without sudden movements generated by wind gusts. Affecting the flight attitude of the UAV by more than about 8° (especially the κ angle) can lead to the appearance of parallax in stereo restitution projects. Other additional systems that have been used to improve the positioning of the system: the professional flight control system, DJI A3 Pro (consisting of three GNSS antennas and three IMU units, which work as a redundant and mutual control system) and the D-RTK positioning system for precise autonomous flights that works on the RTK Base-Rover principle. These additional systems bring a considerable contribution to the flight attitude of the aircraft and mitigates the effects of wind gusts. Thereby, smooth flights are obtained, without sudden movements, without incidents even in the event of errors in the IMU/GNSS sensors (Development Team of DJI, 2018a).

3. Technology for obtaining DG

The proposed technology consists of combining the best calibration methods, acquisition procedures, processing processes, as well as software solutions. Along with these elements, innovative research elements are also added that together lead to obtaining the orthophoto plane by DG and rectified based on LIDAR data.

Pre-calibration of the LIDAR-Optic system

The first phase of rigorous calibration involved accurately determining the offsets between the IMU sensor and the GNSS antenna, respectively the LIDAR and optical sensors. Calibration was performed by geometric measurement methods after a thorough research of the coordinate systems and their origins, with a maximum error of ±1-2 mm.

Pre-calibration of the IMU-GNSS assembly consisted in determining the offsets between the IMU system and the GNSS antenna, and was performed along the axes of the IMU system (body frame). The determination of the offsets was made from the center of the system to the phase center of the GNSS antenna, by summing the measured segments (Table 1). In addition, transition rotations between theoretical systems that are involved in post-processing have been introduced in Table 1.

Pre-calibration of the IMU-Camera assembly (Sony A7RII) involved the determination of offsets to the perspective center of the camera, considering the lens focal length of approximately 21 mm. The offsets and their determination errors are consolidated in Table 2. Table 2 also centralized the initial rotations between the IMU and the camera coordinate system, which are to be rigorously calibrated.

Pre-calibration of the IMU-LIDAR assembly (Velodyne Ultra Puck VLP 32c) involved determining the offsets to the optical center of

the LIDAR sensor. The determined offsets were centralized in Table 3, alongside the initial rotations between the PLS systems (LIDAR) and the IMU sensor. They will be rigorously calibrated through specialized procedures and software for each individual laser head.

Air data enhancement

To obtain photogrammetric products through DG, it is necessary to take into account a multitude of factors that affect accuracy throughout the entire data acquisition process. In addition to rigorous system calibration, it is necessary to use best practices in photogrammetric data acquisition. Along with these, there are other principles and methods that can help eliminate certain errors and consequently improve aerial data.

Ensuring smooth flight is a basic requirement in obtaining quality photogrammetric data. Although the UAV system uses a precise positioning system (D-RTK GNSS system), the flight assurance is given by the integration of several data. Thus, along with GNSS data, the IMU sensors and the magnetic compass play an important role in the stability and uniformity of a flight. The IMU sensors are calibrated whenever large differences are found between the three modules installed on the flight platform. The IMU calibration should be performed in an area with flat terrain (Development Team of PLS, 2019). Magnetic compass calibration is performed much more often, basically every time the flight location is more than 30 km away from the last calibration performed (Development Team of PLS, 2019). The variation of gravity from one area to another, but also electromagnetic interference led to the need to calibrate this sensor quite often. In the absence of this calibration, chaotic movements can be encountered in the flight of the drone (Development Team of DJI, 2018b).

The optimal scanning method is based on autopilot flight, based on a flight design that has been conceived using the stated principles. One of the most versatile autonomous flight applications, Litchi, was used in this regard. In the case of LIDAR data acquisition, it is very important that the scan is performed on straight trajectories, as errors occur in the case of curves or sudden changes in direction.

The optimal method of aerial photography in the case of DG is defined by a side coverage of more than 55% and a forward overlap of more than 80% (Ma et al., 2020). This coverage generates accurate image correlation with a major impact on DG accuracy, even for classical photogrammetry (Gruber et al., 2022).

Table 1. IMU-GNSS offsets and rotations between theoretical coordinate systems

The coordinate system	X axis	Y axis	Z axis	RMS_X	RMS_Y	RMS_Z	Mentions
Offsets in Coordinate System of IMU to GNSS	-0.019m	0.050m	0.369m	0.002m	0.002m	0.001m	Used in post-processing (PP) (Inertial Explorer)
IMU Body Frame Rotations -> Vehicle Body F.	-90°	0°	0°	-	-	-	Used in post-processing (PP) (Inertial Explorer)

Table 2. IMU-Camera Sony A7RII offsets and initial rotations between IMU-Camera systems

The coordinate system	X axis	Y axis	Z axis	RMS_X	RMS_Y	RMS_Z	Mentions
Offsets in the IMU Coordinate System to Camera	-0.019m	0.141m	0.042m	0.002m	0.002m	0.003m	Used in post-processing (PP) (Inertial Explorer)
IMU Body Frame Rotations -> Camera Frame	0°	0°	0°	-	-	-	Used in PP. Extrinsic rot. X, Y, Z (Inertial Explorer)

Table 3. IMU-LIDAR VLP 32c offsets and initial rotations between systems

The coordinate system	X axis	Y axis	Z axis	RMS_X	RMS_Y	RMS_Z	Mentions
Offsets from IMU Coordinate System to the PLS System (LIDAR)	-0.019m	0.046m	0.043m	0.001m	0.001m	0.001m	Used in PP and real-time (Spatial Explorer)
SPAN IMU Body Frame Rotations -> LIDAR Frame	-45°	90°	90°	-	-	-	Used in PP and real-time. Extr. rot. Z, X, Y (Spatial Explorer)

Atmospheric influences are another important aspect in DG. The most important elements that can negatively affect flight missions are represented by wind gust speed (>5 m/s) and the *Kp* index of geomagnetic storms (>3). The geomagnetic storms that induce significant errors in the magnetic field of the planet, and in the waves that cross the ionosphere fall within the 4-9 *Kp* range (Matzka, 2023). The index of geomagnetic storms on the surface of the planet, *Kp*, is of particular importance because it induces errors in GNSS positioning, in radio transmissions, in any electronic sensor, and consequently in the UAV flight attitude (Development Team of NOAA, 2023).

The RTK corrections provided a priori PPK (Post Processing Kinematics) generated improved results in terms of the quality of the flight trajectories.

Trajectory calibration is accomplished in two stages: *static* and *kinematic* alignment (Development Team of NovAtel, 2019b). The *static alignment* was achieved by two sessions of static satellite measurements, one at the beginning of the flight and one after its completion. Static sessions required the drone to remain stationary for at least 10 minutes, clear of obstacles and with the engines off, during which satellite data was recorded every second (Development Team of PLS, 2021).

For systems equipped with only a GPS antenna, the IMU calibration procedure is completed by *kinematic alignment*. The first part of the calibration was performed through a straight flight, at a speed of over 6m/s, carried out in the direction of the wind, in the opposite direction. The second part of the airborne calibration consisted of calibrating the IMU with the GNSS data. IMU sensors are affected by drift errors, directly proportional to time passed from initial calibration (Development Team of NovAtel, 2020), therefore they are correlated with the position of the GNSS antenna. This calibration consisted of performing movements in the air (infinity shaped movements ∞), that involves large variations on each of the three components: *yaw*, *pitch*, *roll*. A minimum of 3 infinity shapes are required, until a relative calibration of the data recorded by the IMU sensor is achieved in the arcsecond range (Development Team of PLS, 2023). Since the PPK is performed in *forward*/*reverse* mode, all these procedures must be done in the mirror at the end of the flight mission. IMU calibration deteriorates over time in straight flights, even when it is correlated with precise GNSS positioning and corrected by the intelligent SPAN system (Development Team of NovAtel, 2019a). For this reason, it is recommended to limit the acquisition of photogrammetric data to strips of approximately 1 km, with block flights being preferable, not strips. The IMU sensor will recalibrate with each turn to the next lane due to the large variations in the three components: *yaw*, *pitch* and *roll*.

4. Experimental data: Isaccea Port

Based on the flight realised in the new Isaccea Port, both the rigorous calibration procedure and the obtaining of DG data were accomplished. The flight performed in Isaccea port was designed for the calibration of the LIDAR and camera sensors. The design of the flight assumed the creation of several sets of flight lines (in both directions), perpendicular to each other and with a 55% side coverage and 85% forward coverage (Terrasolid Ltd, 2022). After the flight, 23 GCPs were measured for the orthophoto plan and 29 points for the LIDAR data. The 23 GCPs will be exploited to calibrate the camera used, but also to check the DG.

PPK of the flight trajectory

Flight trajectory post-processing (PPK) was performed with the Inertial Explorer software solution, developed by NovAtel. As the GNSS and IMU data were of high quality, they were *tightly coupled* in the PPK process. Data processing was performed using a fixed base, with satellite records at one-second, using the European Terrestrial Reference System 1989 (ETRS89) datum the ETRS2000 frame, at epoch 2000. Accurate satellite ephemerides were used, trajectory quality being critical for DG. As results after PPK, differences between *forward*/*reverse* solutions of less than 3 mm in the horizontal plane and less than 12 mm in the vertical plane were obtained. From the point of view of the angles that define the attitude of the UAV, the differences between the *forward*/*reverse* solutions were a maximum of 0.6 arcminutes on each component. Finally, the two solutions were combined, resulting the final trajectory. The application was configured to

export the external orientation angles ω, φ, κ of the images relative to the national coordinate system, Stereographic 1970 (Zhao et al., 2014). The coordinates were adjusted with the offsets determined in Table 2 and then transformed into the national coordinate systems of Romania, with the TransDatRo v4.06 application.

Internal camera calibration

Image processing was done with the PIX4D Mapper software solution. The procedure used for internal camera calibration is BBA, using Automatic AeroTriangulation (AAT) techniques and GCP (Christian Heipke, 2002). The BBA was performed with an accuracy of 6 mm on X and Y axes, and of 17 mm on the Z axis. For a correct analysis, it should be noted that the average value of the GSD is 15.4 mm. Interchangeable lenses of non-metric cameras are not precisely calibrated in terms of focal length, optical center, radial or tangential distortions. Internal orientation parameters are sensitive to exposure from the acquisition environment, to extreme temperatures, pressure or vibrations (Oniga & Maximilian, 2013). Furthermore, a rigorous calibration done in the laboratory does not deliver the best results (Yodono Garcia et al., 2020), even less in a DG process. The distortions produced by lens aberrations (radial, tangential), also prevent the use of images in stereo restitution projects. Taking images with UAV systems from low altitude, amplifies parallax due to distortions and prevents the creation of stereoscopic models. This is the reason why non-metric cameras must be calibrated in the environment where are used, and then easily recalibrated within each mission. The laboratory calibration was used as a priori data, resulting the calibrated interior orientation parameters (Figure 1).

In order to verify the previously stated principles, the 23 GCPs were used as CPs (Check Points). DG processing was performed both with the laboratory calibrated camera and with the camera calibrated through the AAT and BBA process. The errors obtained in this first phase of DG are presented in Table 4. The analysis of Table 4 reveals that a laboratory camera calibration can be used to obtain orthophoto plans with average accuracy, relative to GSD. The visible difference between the obtained results demonstrates the high quality of the calibration achieved by the BBA process.

Camera boresight calibration

The rotations between the IMU sensor and the Sony A7RII camera determined in Table 2 must be rigorously calibrated. Uncalibrated orientations can be automatically corrected by the AAT process. However, a rigorously calibrated optical sensor with the IMU sensor translates into much more accurate image orientation data in the AAT process. The main effect of this rigorous calibration is to reduce the time to identify the tie points between the images, and to mitigate the risk of them being incorrectly identified (Ciobanu et al., 2022). Starting from the ω, φ, κ angles calculated in the BBA process, the correction angles (boresight) were calculated with NovAtel Inertial Explorer.

	Focal Length	Principal Point x	Principal Point y	R1	R2	R3	T1	T2
Initial Values	4723.510 [pixel] 20.790 [mm]	3990.200 [pixel] 17.563 [mm]	2648.330 [pixel] 11.656 [mm]	-0.013	0.013	-0.005	0.000	0.000
Optimized Values	4715.848 [pixel] 20.756 [mm]	4010.424 [pixel] 17.652 [mm]	2651.175 [pixel] 11.669 [mm]	-0.014	0.013	-0.005	-0.000	0.001
Uncertainties (Sigma)	0.279 [pixel] 0.001 [mm]	0.073 [pixel] 0.000 [mm]	0.073 [pixel] 0.000 [mm]	0.000	0.000	0.000	0.000	0.000

Figure 1. Capture from BBA report (PIX4D Mapper) - Sony A7RII internal orientation parameters calibration

Table 4. DG comparison using internal orientation parameters calibrated in laboratory or by BBA

Statistical Indicator	LABORATORY CALIBRATION			BBA CALIBRATION		
	Error X [m]	Error Y [m]	Error Z [m]	Error X [m]	Error Y [m]	Error Z [m]
Mean [m]	0.0125	0.0125	0.1171	0.0023	-0.0078	0.0060
Sigma [m]	0.0241	0.0215	0.0321	0.0084	0.0076	0.0192
RMS Error [m]	0.0271	0.0249	0.1214	0.0087	0.0108	0.0201

The algorithm for boresight calibration is based on the rotation equation from the image to the terrain coordinate system. The calculation of the corrections was realized in accordance with the definition of the Stereographic 1970 coordinate system. After the boresight calibration, the whole process of AAT was repeated. Figure 2 shows a graphical comparison between the quality of the BBA performed before and after the boresight calibration.

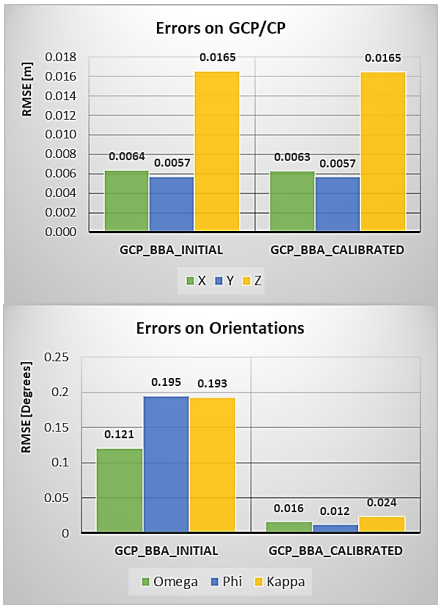

Figure 2. The influence of boresight calibration of the Sony A7RII camera in the BBA process

From the analysis of the graphs in Figure 2, it can be seen that the positioning errors on GCPs remain approximately identical. The errors obtained on the orientations after the rigorous calibration of camera are ten times smaller. This translates into an efficiency in the AAT process.

Rigorous calibration of the LIDAR sensor

Orthorectification of photogrammetric data using LIDAR data requires a high quality of these data. In the case of the present study, the flight was designed in an area with roads, platforms, concrete walls, beams, etc., for a better calibration of the LIDAR data. The software solution used to determine the correction angles for each laser heads was the TerraScan and TerraMatch application developed by Terrasolid Ltd. Starting from the rotations determined in Table 3, LIDAR data was exported for each individual laser head. The final objective of the calibration involves the calculation of the correction angles on all three axes: *heading* (*-yaw*), *pitch*, *roll*. The LIDAR point cloud was noise filtered and then classified into object classes on each strip and laser head. After classifying the LIDAR data, matching lines were identified in each set, lines that approximate very well certain areas on the ground, buildings, or walls. Matching lines are used to calculate corrections on each rotation axis (Terrasolid Ltd, 2022). A total of approximately one hundred thousand cross-sections with matching lines were used in the calibration process. As previously specified, laser head calibration for the IMU-Velodyne VLP 32c system was initially performed in a work-specific environment by the system integrator Phoenix LiDAR Systems LLC. Following the current calibration, the analysis of the corrections obtained on the three angles shows a good initial calibration, with the corrections having insignificant values. Checking the statistical parameters before and after calibrating the laser heads reveals only a small improvement in the quality of LIDAR data (Table 5). It should be pointed out that these calibrations are also limited by the constructive accuracy of the LIDAR sensor (±3cm, under optimal conditions).

In the case of the LIDAR calibration, the data were used in the ETRS89 coordinate system, using the Universal Transverse Mercator (UTM) 35N projection. In addition to the LIDAR point cloud, PPK trajectories were also used, with the obtained accuracies. Because flight trajectories have atypical formats, they are difficult to convert to other coordinate systems which are not based on GRS80, without a loss of accuracy.

Table 5. Verification of statistical parameters before and after LIDAR data calibration

LIDAR Verified	Check on GCP [m]					Check on strips [m]
	Average dZ	Min. dZ	Max. dZ	1 Sigma	RMSE	Avg. Magnitude
INITIAL	0.017	-0.012	0.047	0.015	0.022	0.0229
CALIBRATED	0.017	-0.016	0.042	0.013	0.022	0.0223

Therefore, in the case of LIDAR data, the export is first done in the UTM system and after calibration the LIDAR data is transformed in others systems.

Preliminary results of DG

The photogrammetric data were reprocessed, using the calibrated interior and exterior orientation elements. The data were processed using the principle of DG. Thus, GCPs were used only as CPs to be able to evaluate the final quality of the obtained data. The obtained accuracies were compared with the classical way of generating orthophoto plans (BBA), but also with the accuracy of DG obtained with PPK trajectory, but uncalibrated sensors (DG PPK). From the analysis of Figure 3, it can be concluded that satisfactory accuracy can be obtained through DG if the stated principles and working method detailed in this study are followed. If the sensors are rigorously calibrated, then with DG accuracies similar to the BBA technology can be achieved.

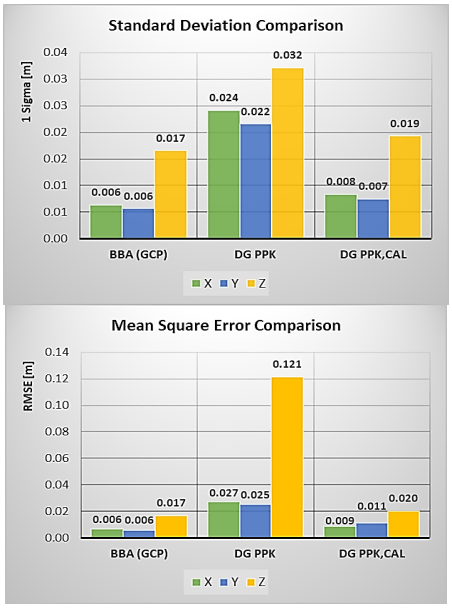

Figure 3. Comparison of the quality of Direct Georeferencing obtained after rigorous calibration

It should be emphasized that the accuracies obtained in BBA are substantially improved by using images with high overlap: over 50% side overlap, respectively over 85% forward overlap.

5. Precise transformation of LIDAR data

Orthorectification is currently performed based on the tie points dense cloud generated through the AAT process. Until now, there was no possibility to use LIDAR data to orthorectify images, with the aim of obtaining orthophoto plans in the National Projection System, Stereographic 1970. One of the impediments was the lack of precision of the LIDAR data obtained by DG, but which can be solved by rigorous calibration and the stated principles. The second significant impediment in the specific case of Romania consists in the lack of a precise transformation of the LIDAR data in the national coordinate systems. The problem of transformation from the ETRS89 geodetic system (based on GRS80 ellipsoid) to the Stereographic 1970 oblique azimuthal projection system (having associated Krasovski datum 1942 and Krasovski 1940 ellipsoid) has been solved for point transformations (Avramiuc et al., 2009), but it is difficult to apply for atypical data formats. The situation becomes even more complicated when the transformation of ellipsoidal heights into normal heights, referred to the Black Sea 1975, is performed. This system of normal heights is based on a continuously developing quasi-geoid (Avramiuc et al., 2019), which further complicates matters by periodically releasing new transformation parameters (The National Center for Cartography, 2020).

The errors obtained by transforming the LIDAR data with the generic software range from decimeters to meters, both planimetrically and in elevation. In this context, together with other researchers, we developed the RoTLAS APP v1.62 for high-precision transformation of LIDAR data into LAS format. Consequently, the acquired LIDAR data were transformed into national coordinate systems with an accuracy identical to the TransDatRo v4.06 application. The differences between a point transformation performed with the official app and RoTLAS APP v1.62 are sub-millimeter and essentially represent residual errors (Ilie et al., 2022).

RESULTS AND DISCUSSIONS

1. DG orthophoto plan, rectified on LIDAR data: Isaccea Port

The calibrated and precisely transformed LIDAR point cloud in the Stereographic 1970 system, respectively Black Sea 1975, was used as a substitute for the dense cloud of tie points. The orthophoto mosaic made by DG is presented in Figure 4, superimposed with the GCPs (R4 and R6 are detailed).

The accuracy obtained by direct georeferencing is presented in Figure 3 (section DG PPK, CAL). The quality of the orthorectification is presented by comparison in Figure 5. No discrepancies were identified between the georeferencing of the optical data and the LIDAR data, a fact also demonstrated by the correct orthorectification.

Improvements in orthorectification are found in areas shaded by vegetation and in the case of atypical structures such as communication antennas, where classical orthorectification fails. For projects where both optical and LIDAR data are required, a considerable time saving of approximately 54% can be achieved using LIDAR data. The time saved multiplies by the number of flights involved in the project, to which is added the time saved that would have been necessary for determining the GCP.

2. Validation of DG: Turnu Magurele Port

The validation of the DG was carried out based on two new flights performed in Turnu Magurele Port. The calibrated internal orientation parameters of the camera (Figure 1) were easily recalibrated to the new environmental conditions of the current project (as close as possible to the initially calibrated data). The internal orientation parameters of DSLR cameras are sensitive to exposure from the acquisition environment, to extreme temperatures, pressure or vibration (Yodono Garcia et al., 2020), which is why slight corrections are required. To fully validate the proposed procedure, the quasi-geoid model used has also changed: TransDatRo version v4.07 (Bagherbandi et al., 2022).

Validation of DG accuracy on CP

To check the DG against the classical method, 17 GCPs were determined. Also, 132 RTK points were determined in the normal working mode, to verify the stereo restitution projects realised with DG. In a first step, the accuracies obtained by the two BBA and DG methods were compared (Figure 6).

Figure 4. Direct georeferenced orthophoto plan, orthorectified based on LIDAR data

Figure 5. Comparison between classical (left) and on LIDAR data (right) orthorectification

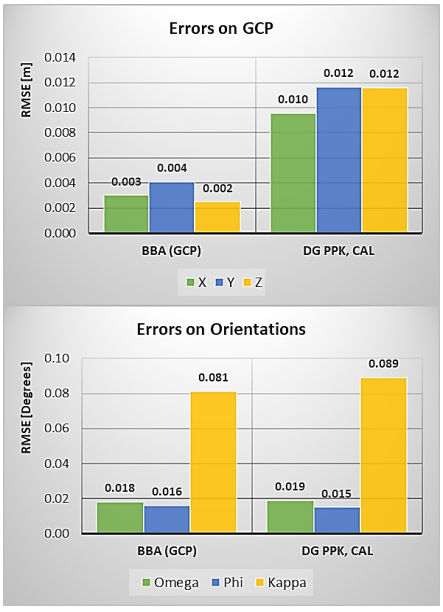

Figure 6. Validation of DG based on statistical data

The inputs to the BBA process were the high-coverage images (taken as for DG) and the calibrated camera. Thereby, the accuracies obtained by BBA were also improved. The DG was carried out in a similar way to the one presented in case of Isaccea Port.
The data in Figure 6 highlights the fact that the errors on each axis were below the value of 1 GSD of 14.4 mm. From the point of view of errors on the orientations, a slight systematic influence of the wind (the value of the angle κ) is found. This error has no influence on the georeferencing accuracy for photogrammetric data, due to the AAT process present in both processing modes (BBA/GD). In conclusion, it can be noticed that the goal of obtaining directly georeferenced products within the accuracy limit of 1-2 GSD has been achieved.

Validation of orthorectification on LIDAR

In order to validate the orthorectification mode, the orthophoto plan made in the classical way (BBA) was compared with the orthophoto plan made based on the LIDAR point cloud. The verification was carried out on several classes of objects. The first check was carried out on buildings, with an emphasis on areas covered by vegetation. In Figure 7 two types of buildings were chosen: with roof in two waters (extended to the walls) and respectively with a terrace roof. In the classic process carried out by AAT, orthorectification errors were identified, especially in areas covered by vegetation, but also in the case of buildings with terraced roofs. Using orthorectification based on LIDAR data, these errors were eliminated. Moreover, the LIDAR orthorectification of building edges was found to be less jagged and closer to the reality.

Figure 7. Buildings and vegetation: the improvement brought by orthorectification based on LIDAR data

The second way of validating DG with LIDAR orthorectification, was performed on a telecommunications antenna. Orthorectification based on the dense point cloud generated by AAT completely fails for atypical structures (Figure 5, left). Significant improvements are found in antenna orthorectification on LIDAR data, but some residual image mosaicking errors remain (Figure 8, right).

Figure 8. Telecommunication antennas: differences between classical and LIDAR orthorectification

For suspended buildings, better results were found on the edges of orthorectified buildings using LIDAR data. In the case of conveyor belts, orthorectification errors were identified with the AAT method, the largest being found in the case of uncovered conveyor belts (Figure 9).

Figure 9. Suspended buildings: differences between classical and LIDAR orthorectification

Industrial machines are also difficult to orthorectify, because they are composed of atypical structures, partially suspended in the air (Figure 10).

Figure 10. Industrial machinery: differences between classical and LIDAR orthorectification

Through the classic orthorectification technology (Figure 10, left) the results are completely unusable. Figure 10 exemplified the case of a wharf crane, which is substantially better orthorectified by the DG procedure on LIDAR data (right image). Also, in this case there are small mosaic errors that can be rectified by manual editing of the orthophoto plane. Better results can be achieved if these

atypical machines are scanned from four different directions. Usually, their rectification is not of great interest. If the project is carried out in areas such as refineries, mining excavations, chemical plants, then the rectification of atypical objects is necessary.
Classic orthorectification was positively influenced by the high coverage between the acquired images. The good results obtained based on LIDAR data rectification are also due to the high density of points per square meter, with an average of over 550 points/m^2.

3D validation of DG by stereo restitution

The final part of the validation was performed by stereo restitution, to verify the accuracy of the DG process in a three-dimensional system. In order to be able to perform stereo restitution projects, the images were rectified from the influence of radial and tangential distortions using the internal orientation calibrated parameters. The DG stereo restitution project was verified with the help of the 17 GCPs through stereoscopic measurements (Table 6).
Following the precisions obtained and in accordance with GSD, respectively with the precisions presented for the classical case (Figure 6), the stereo restitution made by the DG process is validated. The orthophoto plane made through DG was also checked with the 3D vector data from the stereo restitution by BBA (Figure 11) and with RTK data from the field.

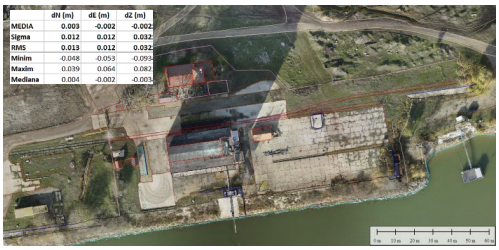

Figure 11. Orthophoto plan verification based on vector data from stereo restitution

To compute the stereoscopic accuracy over the entire validation area from Turnu Magurele Port, 132 points were determined by RTK technology. CPs were chosen on the railways or on the crane's tracks. This type of points is considered to be the most difficult to measure in a stereoscopic model. Figure 11 shows the error statistics of the differences found on the 132 CP. After normalizing the observed differences, they were represented graphically in order to analyze their distribution (Figure 12).

Table 6. Direct georeferencing verification by GCP reading through stereo restitution

No. PTS	PTS NAME	Coordinate systems: Stereographic 1970, Black Sea 1975, Ed. 1990 - RTK MEASUREMENTS			Coordinate systems: Stereographic 1970, Black Sea 1975, Ed. 1990 - DG STEREORESTITUTION			Measurement Differences RTK-DG		
		North (m)	East (m)	Elev. (m)	North (m)	East (m)	Elev. (m)	dN	dE	dH
1	CB1	246204.109	491995.281	25.823	246204.082	491995.283	25.805	0.027	-0.002	0.018
2	CB2	246033.325	491553.281	25.689	246033.327	491553.277	25.680	-0.002	0.004	0.009
3	CB3	246130.565	492074.477	26.265	246130.572	492074.474	26.252	-0.007	0.003	0.013
4	CM1	246046.764	491256.538	27.417	246046.747	491256.554	27.397	0.017	-0.016	0.020
5	R1	246098.203	492004.645	25.654	246098.201	492004.641	25.637	0.002	0.004	0.017
6	R10	245897.748	491324.338	22.459	245897.751	491324.338	22.433	-0.003	0.000	0.026
7	R11	245999.607	491241.164	26.996	245999.605	491241.158	26.987	0.002	0.006	0.009
8	R12	245982.928	491314.693	27.109	245982.917	491314.692	27.091	0.011	0.001	0.018
9	R13	246046.433	491586.885	25.404	246046.428	491586.870	25.392	0.005	0.015	0.012
10	R2	246139.846	492073.387	26.342	246139.841	492073.384	26.328	0.005	0.003	0.014
11	R4	246188.000	492329.869	23.848	246187.994	492329.864	23.844	0.006	0.005	0.004
12	R5	246294.850	492178.513	26.827	246294.848	492178.530	26.812	0.002	-0.017	0.015
13	R6	246193.761	492106.337	25.983	246193.736	492106.341	25.987	0.025	-0.004	-0.004
14	R7	246062.406	491770.006	26.279	246062.403	491769.989	26.281	0.003	0.017	-0.002
15	R8	246119.681	491684.352	26.551	246119.668	491684.346	26.554	0.013	0.006	-0.003
16	R9	245947.838	491498.857	25.576	245947.845	491498.838	25.572	-0.007	0.019	0.004
17	TM1	246066.428	491780.939	26.249	246066.432	491780.917	26.229	-0.004	0.022	0.020
							Media	**0.006**	**0.004**	**0.011**
							Sigma	**0.010**	**0.010**	**0.009**
							RMS	**0.011**	**0.011**	**0.014**

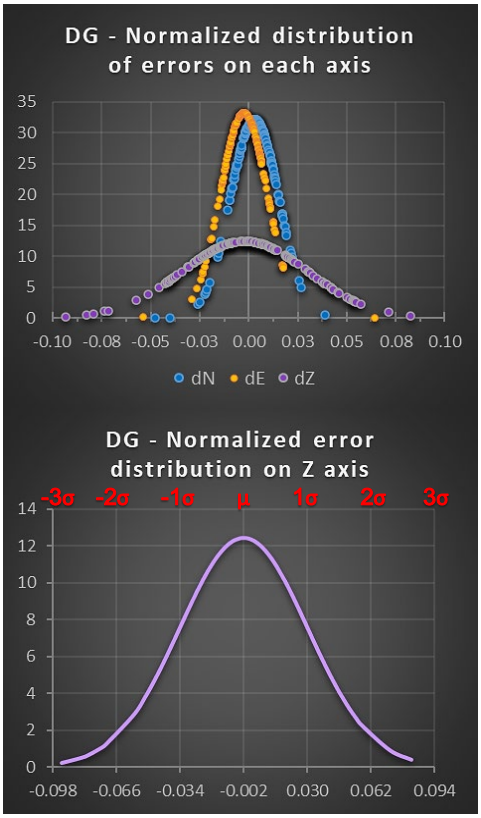

Figure 12. Normalized distribution of errors on 132 CP

Most planimetric differences fall within ±36 mm, which is close to the error of the RTK point determination method. In terms of the differences identified on hight, they are larger, but evenly distributed. The dispersion of errors on the Z-axis is in contrast with the dispersion of errors obtained on the Z-axis from GCP. From the point of view of stereo restitution, the only major difference between the checkpoints is the ease with which they can be scored in the stereoscopic model. In conclusion, an influence generated by the human eye is found, which manifests itself equally in both directions. Thus, the human eye can limit the accuracy of data acquired by stereo restitution, despite the very small size of the GSD.

CONCLUSIONS

The research carried out in the field of DG in the coordinate systems of Romania brings with it several benefits. The most important benefits are production time efficiency and cost reduction associated with photogrammetric products. Orthorectification based on LIDAR DG data is performed much more accurately in many situations and brings more efficiency in the creation of orthophoto plans. As a result of this research, it was found that the creation of topographic plans by UAV stereo restitution is much faster than classic measurements.

The validation of the DG was carried out on two different versions of the quasi-geoid (version 4.06, respectively version 4.07), the results being similar. The verification of the correctness of the DG was realised by several methods, resulting in a heterogeneous validation. The generated orthophoto plan and the vector plan made by stereo restitution were mutually verified demonstrating the reliability of the procedure. The statistics of these checks highlight the quality of the products made by direct georeferencing.

An aspect that can be improved in future research is the residual mosaicking errors that appear after the rectification based on LIDAR data. This happens especially in the areas of atypical objects. However, orthorectification is performed much more correctly than by classical methods, leaving only mosaic errors to be rectified.

Despite the results obtained, the DG method should be applied with caution. During the production process, random errors may occur that are difficult to identify. For this reason, it is recommended to use 2-3 GCPs to ensure the verification of the entire process.

ACKNOWLEDGEMENTS

The validation by stereoscopic measurements was performed independently with the help of several professional stereo restitutors from the Tehnogis Grup SRL company. The applications used were provided by Tehnogis Grup SRL, Prosig Expert SRL and the Technical University of Civil Engineering of Bucharest. Finally, we thank all those who directly or indirectly supported this research.

REFERENCES

Avramiuc, N., Dragomir, P. I., Rus, T. (2009). Algorithm for direct and inverse coordinate transformation

between ETRS89 CRS and S-42 CRS. *RevCAD Journal of Geodesy and Cadastre*, 105-114.

Avramiuc, N., Erhan, C., Spiroiu, I., Crişan, R.-D.-N., & Flueraş, M. (2019). Determination of a new gravimetric quasigeoid for Romania. *Journal of Geodesy, Cartography and Cadastre*.

Bagherbandi, M., Jouybari, A., Nilfouroushan, F., & Ågren, J. (2022). Importance of Precise Gravity Field Modeling in Direct Georeferencing and Aerial Photogrammetry: a Case Study for Sweden. *The International Archives of the Photogrammetry, Remote Sensing and Spatial Information Sciences, XLIII-B2-2022*, 15-20. doi:10.5194/isprs-archives-XLIII-B2-2022-15-2022

Chiang, K.-W., Tsai, M.-L., & Chu, C.-H. (2012). The Development of an UAV Borne Direct Georeferenced Photogrammetric Platform for Ground Control Point Free Applications. *12*(7), 9161-9180.

Christian Heipke, K. J. a. H. W. (2002). *Integrated Sensor Orientation - Test Report and Workshop Proceedings*. European Organization for Experimental Photogrammetric Research, Vol. Official Publication No 43. (pp. 302).

Ciobanu, D., Kemper, G., Ilie, D., Răducanu, D., & Balotă, O. L. (2022). Using the Open Skies multi sensor system for military observation missions and civilian applications. *Int. Arch. Photogramm. Remote Sens. Spatial Inf. Sci., XLIII-B1-2022*, 301-308. doi:10.5194/isprs-archives-XLIII-B1-2022-301-2022

Correia, C. A. M., Andrade, F. A. A., Sivertsen, A., Guedes, I. P., Pinto, M. F., Manhães, A. G., & Haddad, D. B. (2022). Comprehensive Direct Georeferencing of Aerial Images for Unmanned Aerial Systems Applications. *22*(2), 604.

Development Team of DJI. (2018a). A3 Flight Controller. Retrieved from https://www.dji.com/a3

Development Team of DJI. (2018b). Matrice M600 PRO User Manual. Retrieved from https://dl.djicdn.com/downloads/m600%20pro/1208EN/Matrice_600_Pro_User_Manual_v1.0_EN_1208.pdf

Development Team of NOAA. (2023). Planetary K-Index. Retrieved from https://www.swpc.noaa.gov/products/planetary-k-index

Development Team of NovAtel. (2007). NovAtel SPAN Aerial Photogrammetry Test Flights Results.

Development Team of NovAtel. (2019a). OEM7 on SPAN Installation and Operation User Manual.

Development Team of NovAtel. (2019b). Waypoint Products Group - A NovAtel Precise Prositioning Product [User Manual v8.80]: Hexagon, NovAtel Inc.

Development Team of NovAtel. (2020). SPAN - Tightly coupled GNSS+INS technology for exceptional continuous 3D position, velocity & attitude performance. Calgary, Alberta, Canada: Hexagon, NovAtel Inc.

Development Team of NovAtel. (2022). Antennas Pinwheel OEM. Retrieved from https://hexagondownloads.blob.core.windows.net/public/Novatel/assets/Documents/Papers/Pinwheel_OEM/Pinwheel_OEM.pdf

Development Team of PLS. (2018). Ground Control Recommendation for Phoenix Clients.

Development Team of PLS. (2019). LiDAR Mapping Systems - Drone Pilot Training.

Development Team of PLS. (2021). Post Processing - Workflow with Inertial Explorer and TerraSolid.

Development Team of PLS. (2023, January 19, 2023). Phoenix LiDAR Systems User Manual. Retrieved from https://docs.phoenixlidar.com/

Essel, B., McDonald, J., Bolger, M., & Cahalane, C. (2022). Initial Study Assessing the Suitability of Drones With Low-Cost GNSS And IMU for Mapping Over Featureless Terrain Using Direct Georeferencing. *The International Archives of the Photogrammetry, Remote Sensing and Spatial Information Sciences, XLIII-B2-2022*, 37-44. doi:10.5194/isprs-archives-XLIII-B2-2022-37-2022

Gómez-Gutiérrez, Á., Sánchez-Fernández, M., and de Sanjosé-Blasco. (2022). Performance of Different UAS Platforms, Techniques (LIDAR and photogrammetry) and Referencing Approaches (RTK, PPK or GCP-based) to Acquire 3D Data in Coastal Cliffs. *EGU General Assembly 2022, Vienna, Austria*. doi: https://doi.org/10.5194/egusphere-egu22-9881

Gruber, M., Schachinger, B., & Mostafa, M. (2022). The Next Generation Vexcel Imaging 3D City Modelling Using Directly Georeferenced Data. *The International Archives of the Photogrammetry, Remote Sensing and Spatial Information Sciences, XLIII-B1-2022*, 309-316. doi:10.5194/isprs-archives-XLIII-B1-2022-309-2022

Haala, N., Kölle, M., Cramer, M., Laupheimer, D., & Zimmermann, F. (2022). Hybrid Georeferencing of Images and LiDAR Data for UAV-based Point Cloud Collection at Millimetre Accuracy. *ISPRS Open Journal of Photogrammetry and Remote Sensing, 4*, 100014. doi:https://doi.org/10.1016/j.ophoto.2022.100014

Hutton, J., Lipa, G., Baustian, D., Sulik, J., & Bruce, R. (2020). High Accuracy Direct Georeferencing of the Altum Multi-Spectral UAV Camera and its Application to High Throughput Plant Phenotyping. *ISPRS - International Archives of the Photogrammetry, Remote Sensing and Spatial Information Sciences, XLIII-B1-2020*, 451-456. doi:10.5194/isprs-archives-XLIII-B1-2020-451-2020

Ilie, D., Balotă, O. L., Iordan, D., & Nicoară, P. S. (2022). Algorithm and application development for precise and accurate transformation of LIDAR point clouds into national coordinate systems of Romania using official equations and quasigeoid model. *ISPRS Ann. Photogramm. Remote Sens. Spatial Inf. Sci., V-4-2022*, 181-188. doi:10.5194/isprs-annals-V-4-2022-181-2022

Kordić, B., Gašparović, M., Lužar Oberiter, B., Đapo, A., & Vlastelica, G. (2020). Spatial Data Performance Test of Mid-cost UAS with Direct Georeferencing. *Periodica Polytechnica Civil Engineering, 64*(3), 859-868. doi:10.3311/PPci.15619

Liu, X., Lian, X., Yang, W., Wang, F., Han, Y., & Zhang, Y. (2022). Accuracy Assessment of a UAV Direct Georeferencing Method and Impact of the Configuration of Ground Control Points. *6*(2), 30.

Ma, H., Ma, H., Liu, K., Luo, W., & Zhang, L. (2020). Direct Georeferencing for the Images in an Airborne

LiDAR System by Automatic Boresight Misalignments Calibration. *20*(18), 5056.

Matzka, J. (2023). Indices of Global Geomagnetic Activity. Retrieved from https://www.gfz-potsdam.de/en/section/geomagnetism/data-products-services/geomagnetic-kp-index

Oniga, E., & Maximilian, D. (2013). Metric and Non-Metric Cameras Calibration for the Improvement of Real-Time Monitoring Process Results. *Environmental Engineering and Management Journal, 12*, 719-726. doi:10.30638/eemj.2013.088

Przybilla, H.-J., Bäumker, M., Luhmann, T., Hastedt, H., & Eilers, M. (2020). Interaction Between Direct Georeferencing, Control Point Configuration and Camera Self-Calibration for RTK-Based UAV Photogrammetry. *ISPRS - International Archives of the Photogrammetry, Remote Sensing and Spatial Information Sciences, XLIII-B1-2020*, 485-492. doi:10.5194/isprs-archives-XLIII-B1-2020-485-2020

Salas López, R., Terrones Murga, R. E., Silva-López, J. O., Rojas-Briceño, N. B., Gómez Fernández, D., Oliva-Cruz, M., & Taddia, Y. (2022). Accuracy Assessment of Direct Georeferencing for Photogrammetric Applications Based on UAS-GNSS for High Andean Urban Environments. *6*(12), 388.

Teppati Losè, L., Chiabrando, F., & Giulio Tonolo, F. (2020). Boosting the Timeliness of UAV Large Scale Mapping. Direct Georeferencing Approaches: Operational Strategies and Best Practices. *9*(10), 578.

Terrasolid Ltd, Arttu S. (2022). *TerraMatch User's Guide*.

The National Center for Cartography. (2020). Determination of a quasigeoid for the area of Romania. Retrieved from https://www.cngcft.ro/index.php/ro/portofoliu/proiecte-in-lucru/determinarea-unui-cvasigeoid-pentru-zona-romaniei

Thiab, W., & Seker, D. (2022). *Direct and Indirect Georeferencing with a Light-Weight UAV and an RTK UAV*.

Yodono Garcia, M., Oliveira, H., Fernandes, R., & Costa, D. (2020). Evaluation of Different Methods for Non-Metric Camera Calibration. *Anuario do Instituto de Geociencias, 43*, 266-272. doi:10.11137/2020_1_266_272

Zhao, H., Zhang, B., Wu, C., Zuo, Z., Chen, Z., & Bi, J. (2014). Direct georeferencing of oblique and vertical imagery in different coordinate systems. *ISPRS Journal of Photogrammetry and Remote Sensing, 95*, 122-133. doi:https://doi.org/10.1016/j.isprsjprs.2014.06.001